

Resonant state expansion applied to two-dimensional open optical systems

M. B. Doost, W. Langbein, and E. A. Muljarov*

School of Physics and Astronomy, Cardiff University, Cardiff CF24 3AA, United Kingdom

(Dated: April 3, 2024)

The resonant state expansion (RSE), a rigorous perturbative method in electrodynamics, is applied to two-dimensional open optical systems. The analytically solvable homogeneous dielectric cylinder is used as unperturbed system, and its Green's function is shown to contain a cut in the complex frequency plane, which is included in the RSE basis. The complex eigenfrequencies of modes are calculated using the RSE for a selection of perturbations which mix unperturbed modes of different orbital momentum, such as half-cylinder, thin-film and thin-wire perturbation, demonstrating the accuracy and convergence of the method. The resonant states for the thin-wire perturbation are shown to reproduce an approximative analytical solution.

PACS numbers: 03.50.De, 42.25.-p, 03.65.Nk

I. INTRODUCTION

The electro-magnetic spectrum of an open optical system is characterized by its resonances. Optical resonators,¹ such as planar microcavities,² photonic crystal fibers,³ dielectric micro-spheres,⁴ micro-disks^{5,6} and micro-cylinders^{7–9} are examples of such systems designed to have a series of narrow resonances in their optical spectra. Such resonances, known as cavity modes in planar microcavities and whispering gallery modes (WGMs) in micro-spheres and -cylinders, are characterized by their spectral positions and linewidths, given, respectively, by the real and imaginary part of the complex eigenfrequencies of the system.

Finite linewidths of resonances are typical for open systems and are due to energy leakage from the system to the outside. This leakage can be enhanced by various structural imperfections and scatterers. In particular, when an object is placed inside or in close proximity to the cavity, the resulting modification of the electromagnetic susceptibility perturbs the cavity resonances, changing both their position and linewidth, most noticeably for the high-quality (i.e. narrow-line) resonances. This effect is the basis for resonant optical biosensing.^{7,10,11} The changes in the spectral properties of resonators in the presence of perturbations can be used to characterize the size and shape of the attached nanoparticles.^{12,13} The WGM resonances in microdisks and spherical microcavities have been used in sensors for the characterization of nanolayers¹⁴, DNA¹⁵ and protein molecules,¹⁶ as well as for single atom¹⁷ and nanoparticle detection.^{18,19} Other applications of high-quality modes include miniature laser sources^{20–23} and photonic-crystal optical fibers.³

While the eigenmodes of resonators with simple and highly symmetric geometries can in some cases be calculated exactly, determining their perturbations presents a significant challenge as the popular computational techniques in electrodynamics, such as the finite difference in time domain^{24,25} or finite element method^{26–28} need excessively large computational resources both in memory and processor usage.^{29,30} This is due to the ex-

tremely large computational domain in space and time required to model high quality modes. To treat such narrow resonances and their perturbations, we have recently developed³¹ a rigorous perturbation theory called resonant state expansion (RSE) and applied it to planar optical resonators with different perturbations³² as well as to spherical resonators reducible to effective one-dimensional (1D) systems.³¹ We have demonstrated on exactly solvable examples in 1D that the RSE is a reliable tool for calculation of wave numbers and electro-magnetic fields of resonant states (RSs),³² as well as transmission and scattering properties of open optical systems.

In the present work we report an important step in the development of the RSE, extending the method to effectively two-dimensional (2D) systems (i.e. 3D systems translational invariant in one direction) which are *not reducible* to effective 1D systems. We provide a summary of the theory in a general 3D case, apply it to an effective 2D system, and then consider examples which cover several important types of perturbations. We treat an ideal dielectric cylinder with uniform dielectric constant in vacuum as unperturbed system and calculate perturbed RSs for homogeneous (i.e. reducible to 1D) and inhomogeneous perturbations, including a half-cylinder, thin-film, and thin-wire perturbations. None of these inhomogeneous perturbations have known exact analytic solutions which could be used for verification of the RSE. However, the case of a narrow wire inside a cylinder allows for an approximate analytic solution suitable for weak perturbations.^{33,34} This solution is compared with the present results of the RSE, demonstrating a good agreement.

In the literature, the scattering properties of an open system are often described in terms of a continuum of its eigenstates, all having real frequencies. Such a continuum, together with isolated eigenmodes (e.g. waveguide modes), if they exist in the spectrum, form a mathematically complete set of states suitable for expansions. The continuum, however, presents a significant obstacle for computational methods like perturbation theory, which are based on such expansions. The concept of RSs, naturally following from the observation of resonances in the

spectra of open systems, introduces another complete set of eigenstates which eliminates the continuum from the spectrum, replacing it by a countable number of discrete modes with complex frequencies. This is the basis used in the RSE.

One striking feature of 2D systems, which is revealed in the present work, is the presence of a one-dimensional continuum in the manifold of RSs. This continuum is specific to 2D systems and is required for the completeness of the basis and thus for the accuracy of the RSE applied in 2D as discussed in this work in some detail. Such continua are generally known in the theory of quasi-guided modes in photonic crystal structures³⁵ as potential sources of Wood-Rayleigh anomalies in optical spectra.^{36–40} Technically, they are caused in that case by the presence of square roots in the photon dispersion of light propagated and Bragg scattered inside the photonic crystal. In the case of a dielectric cylinder, which is used for the RSE in 2D, the continuum originates mathematically from the cut in the cylindrical Hankel functions solving Maxwell's equations outside the cylinder.

The paper is organized as follows. In Sec. II we give the general formulation of the RSE for an arbitrary three-dimensional (3D) system. In Sec. III we treat the special case of effective 2D systems using the homogeneous dielectric cylinder as unperturbed system and adding the contribution of the cut to the RSE. This is followed by examples illustrating the method and comparing results with existing analytic solutions. Details of the general formulation of the method, its application in 2D, and the calculation of matrix elements for specific perturbations are given in Appendices A-D.

II. RESONANT STATE EXPANSION

In general, RSs in an open optical system with local dielectric constant $\varepsilon(\mathbf{r})$ and permeability $\mu = 1$, where \mathbf{r} is the three-dimensional spatial position, are the eigen-solutions of the Maxwell wave equation,

$$\nabla \times \nabla \times \mathbf{E}_n(\mathbf{r}) = k_n^2 \varepsilon(\mathbf{r}) \mathbf{E}_n(\mathbf{r}), \quad (1)$$

which satisfy the outgoing wave boundary condition

$$\mathbf{E}_n(\mathbf{r}) \rightarrow r^{-(D-1)/2} e^{ik_n r} \quad \text{for } r \rightarrow \infty, \quad (2)$$

where $r = |\mathbf{r}|$, D is the space dimensionality, k_n is the wave-vector eigenvalue of the RS numbered by the index n , and $\mathbf{E}_n(\mathbf{r})$ is its electric field eigenfunction. The time-dependent part of the RS wave function is given by $\exp(-i\omega_n t)$ with the complex eigenfrequency $\omega_n = ck_n$, where c is the speed of light in vacuum. RSs are either stationary or time-decaying solutions of Maxwell's equation. The wave numbers k_n of time-decaying RSs lie in the lower half of the complex k -plane and come in pairs, having the opposite real and equal imaginary parts. Indeed, if $\mathbf{E}_n(\mathbf{r})$ and k_n corresponding to RS n satisfy Eqs. (1) and (2), taking the complex conjugate of Eq. (1)

we find that $\mathbf{E}(\mathbf{r}) = \mathbf{E}_n^*(\mathbf{r})$ and $k = \pm k_n^*$ also satisfy the same equation. Only $-k_n^*$ has a negative imaginary part as required for time-decaying solutions. We label the resulting RS with index $-n$, so that $k_{-n} = -k_n^*$.

For any open system, the RSs form an orthonormal complete set of eigenmodes. It follows from Eq. (2) that solutions decaying in time grow exponentially in space as $r \rightarrow \infty$. Therefore the normalization of RSs cannot be simply given by the usual volume integrals over their wave functions but it also needs to involve the electromagnetic energy flux through a surface surrounding the system. The orthogonality of RSs for $n \neq m$ has the form

$$0 = (k_n^2 - k_m^2) \int_V d\mathbf{r} \varepsilon(\mathbf{r}) \mathbf{E}_n(\mathbf{r}) \cdot \mathbf{E}_m(\mathbf{r}) - \int_{S_V} dS \left(\mathbf{E}_n \cdot \frac{\partial \mathbf{E}_m}{\partial s} - \mathbf{E}_m \cdot \frac{\partial \mathbf{E}_n}{\partial s} \right), \quad (3)$$

where the first integral in Eq. (3) is taken over an arbitrary volume V which include all system inhomogeneities of $\varepsilon(\mathbf{r})$ while the second integral is taken over the surface S_V surrounding the volume V and contains the gradients $\partial/\partial s$ normal to this surface. This follows strictly from Maxwell's equation Eq. (1) and Green's theorem, using $\nabla \cdot \mathbf{E}_n = 0$ on the surface S_V which is situated outside of the system inhomogeneities. It is convenient, following Eq. (3), to normalize the RSs in the way

$$1 = \int_V d\mathbf{r} \varepsilon(\mathbf{r}) \mathbf{E}_n^2(\mathbf{r}) - \lim_{k \rightarrow k_n} \frac{\int_{S_V} dS \left(\mathbf{E}_n \cdot \frac{\partial \mathbf{E}}{\partial s} - \mathbf{E} \cdot \frac{\partial \mathbf{E}_n}{\partial s} \right)}{k_n^2 - k^2}, \quad (4)$$

where we have used in the second integral an analytic continuation $\mathbf{E}(k, \mathbf{r})$ of the RS wave function $\mathbf{E}_n(\mathbf{r})$ around the point k_n in the complex k -plane. For solutions decaying in time both surface and volume integrals in Eqs. (3) and (4) diverge for $V \rightarrow \infty$. Their superposition, however, removes the divergencies making the normalization independent of V . In the special case of stationary states which are decaying in space, the surface integrals vanish for $V \rightarrow \infty$ and the usual orthonormality in terms of infinite-volume integrals is restored.

The RSE is based on the following three key elements. The *first* one is the Dyson equation,

$$\hat{\mathcal{G}}_k(\mathbf{r}, \mathbf{r}') = \hat{\mathbf{G}}_k(\mathbf{r}, \mathbf{r}') - k^2 \int \hat{\mathbf{G}}_k(\mathbf{r}, \mathbf{r}'') \Delta\varepsilon(\mathbf{r}'') \hat{\mathcal{G}}_k(\mathbf{r}'', \mathbf{r}') d\mathbf{r}'', \quad (5)$$

which relates the perturbed and unperturbed GFs, $\hat{\mathcal{G}}_k$ and $\hat{\mathbf{G}}_k$, respectively. The difference between the perturbed and unperturbed systems is a perturbation of the dielectric constant $\Delta\varepsilon(\mathbf{r})$ with compact support.

The *second* key element is the spectral representation

of the GF,

$$\hat{\mathbf{G}}_k(\mathbf{r}, \mathbf{r}') = \sum_n \frac{\mathbf{E}_n(\mathbf{r}) \otimes \mathbf{E}_n(\mathbf{r}')}{k(k - k_n)} \frac{k_n}{w_n}, \quad (6)$$

which takes into account simple poles of the GF at $k = k_n$ as a sum and a cut of the GF in the complex k -plane as an integral. Details of the derivation of Eq. (6) in a general 3D case, using the Mittag-Leffler and reciprocity theorems, are given in Appendix A, accounting for the tensor form of the GF of Maxwell's equation. The presence of the cut is a specific property of 2D systems having a continuum of RSs in their spectrum. The nature of the cut and its contribution to the RSE is discussed in more detail in Sec. III and in Appendix B. The spectral representation Eq. (6) is used in the Dyson equation (5), for both unperturbed and perturbed systems, equating the residues at the perturbed poles of both sides of Eq. (5). The spectral representation of the unperturbed GF has the normalization constants $w_n = 2k_n$ following from the normalization condition Eq. (4), as shown in Appendices A and B. As for the spectral representation of the perturbed GF $\hat{\mathbf{G}}_k$, in which \mathbf{E}_n and k_n are replaced by \mathbf{E}_ν and k_ν , it is not required by the RSE that the perturbed RSs are normalized in the same way, and thus the corresponding normalization constants can be any.

The *third* element is the completeness of RSs, which is discussed in Appendix A and mathematically expressed by the closure relation Eq. (A9). It allows to expand the perturbed wave functions into the unperturbed ones:

$$\mathbf{E}_\nu(\mathbf{r}) = \sqrt{\varkappa_\nu} \sum_n \frac{c_{n\nu}}{\sqrt{k_n}} \mathbf{E}_n(\mathbf{r}). \quad (7)$$

The expansion coefficients $c_{n\nu}$ are scaled here by $1/\sqrt{k_n}$, in order that the Dyson equation reduces to a linear symmetric matrix eigenvalue problem⁴¹

$$\sum_m \left(\frac{\delta_{nm}}{k_n} + \frac{V_{nm}}{2\sqrt{k_n k_m}} \right) c_{m\nu} = \frac{1}{\varkappa_\nu} c_{n\nu}, \quad (8)$$

in which the matrix elements of the perturbation are defined by

$$V_{nm} = \int \Delta\varepsilon(\mathbf{r}) \mathbf{E}_n(\mathbf{r}) \cdot \mathbf{E}_m(\mathbf{r}) d\mathbf{r}. \quad (9)$$

Equations (7-9), together with the normalization condition Eq. (4) used for the unperturbed modes, define the method called the RSE.

III. APPLICATION TO 2D SYSTEMS

Let us consider systems in 3D space which are homogeneous in one direction (along the unit vector $\hat{\mathbf{z}}$ of the z -axis), and thus can be reduced to effective 2D systems, as their wavevector component along $\hat{\mathbf{z}}$ is conserved and the solution can be separated into a plane wave $\exp(ik_z z)$

and the remaining (x, y) -problem which we express below in polar coordinates $\boldsymbol{\rho} = (\rho, \varphi)$. For such a system, the solutions of Maxwell's equations split into two groups with orthogonal polarizations, called transverse electric (TE) and transverse magnetic (TM), where TE (TM) states have a electric (magnetic) field orthogonal to $\hat{\mathbf{z}}$. This nomenclature relates to the theory of waveguides where the light propagating along $\hat{\mathbf{z}}$ has the dominant component k_z of the wave vector, and the electric (magnetic) field in TE (TM) modes is thus approximately perpendicular to the wave vector. Although we restrict our treatment here to the opposite limit of $k_z = 0$, we follow these adopted notations. In our case, however, the TE (TM) states have the magnetic (electric) field polarization vector strictly parallel to $\hat{\mathbf{z}}$ and thus normal to the wave vector of light at large distances.

We treat in this work only the $k_z = 0$ TM states for which $\mathbf{E}_n = \hat{\mathbf{z}} E_n$ and Eq. (1) reduces to

$$\left[\frac{\partial^2}{\partial \rho^2} + \frac{1}{\rho} \frac{\partial}{\partial \rho} + \frac{1}{\rho^2} \frac{\partial^2}{\partial \varphi^2} + \varepsilon(\rho, \varphi) k_n^2 \right] E_n(\rho, \varphi) = 0. \quad (10)$$

The states are normalized according to Eq. (4) in which the volume V is given by an infinitely long cylinder of radius R . In order to make the normalization constants finite, RSs are normalized per unit length along $\hat{\mathbf{z}}$. The normalization following from Eq. (4) is given more explicitly by³¹

$$1 = \int_0^{2\pi} d\varphi \int_0^R \rho d\rho \varepsilon(\rho, \varphi) E_n^2(\rho, \varphi) + \frac{1}{2k_n^2} \int_0^{2\pi} d\varphi \left[E_n \frac{\partial E_n}{\partial \rho} + \rho E_n \frac{\partial^2 E_n}{\partial \rho^2} - \rho \left(\frac{\partial E_n}{\partial \rho} \right)^2 \right]_{\rho=R_+}, \quad (11)$$

where the last integral is taken over the outer surface of the cylinder. We choose as unperturbed system for the RSE a homogeneous dielectric cylinder in vacuum with radius R and refractive index n_r (which is neither 0 nor 1), having

$$\varepsilon(\rho, \varphi) = \begin{cases} n_r^2 & \text{for } \rho \leq R, \\ 1 & \text{for } \rho > R. \end{cases} \quad (12)$$

Due to the cylindrical symmetry, the azimuthal index m is a good quantum number which takes integer values giving the number of field oscillations around the cylinder. The unperturbed RS wave functions factorize as

$$E_n(\rho, \varphi) = R_m(\rho, k_n) \chi_m(\varphi), \quad (13)$$

where the angular parts are defined by

$$\chi_m(\varphi) = \begin{cases} \pi^{-1/2} \sin(m\varphi) & \text{if } m < 0, \\ (2\pi)^{-1/2} & \text{if } m = 0, \\ \pi^{-1/2} \cos(m\varphi) & \text{if } m > 0, \end{cases} \quad (14)$$

and are orthonormal according to

$$\int_0^{2\pi} \chi_m(\varphi) \chi_{m'}(\varphi) d\varphi = \delta_{mm'}. \quad (15)$$

The choice of the wave functions in the form of standing waves Eq. (14), instead of the more usual $e^{im\varphi}$, is dictated by the general orthogonality condition defined by Eq. (3), without using the complex conjugate. The radial components have the form

$$R_m(\rho, k) = A \begin{cases} J_m(n_r k \rho) / J_m(n_r k R) & \text{for } \rho \leq R, \\ H_m(k \rho) / H_m(k R) & \text{for } \rho > R, \end{cases} \quad (16)$$

in which $J_m(z)$ and $H_m(z) \equiv H_m^{(1)}(z)$ are, respectively, the cylindrical Bessel and Hankel functions of the first kind. The wave functions are normalized according to Eq. (11) with the normalization constant

$$A = \frac{1}{R} \sqrt{\frac{2}{n_r^2 - 1}}. \quad (17)$$

The two boundary conditions at the surface of the cylinder, the continuity of the electric field and its radial derivative, produce a secular equation for the RS wave number eigenvalues k_n , which has the form

$$D_m(k_n R) = 0, \quad (18)$$

where

$$D_m(z) = n_r J'_m(n_r z) H_m(z) - J_m(n_r z) H'_m(z), \quad (19)$$

and $J'_m(z)$ and $H'_m(z)$ are the derivatives of $J_m(z)$ and $H_m(z)$, respectively. Here z represents a complex argument, as opposed to the spatial coordinate used earlier.

The Hankel function $H_m(z)$ which describes the field outside the cylinder and contributes to Eqs. (16) and (19) is a multiple-valued function, or in other words is defined on a Riemann surface having infinite number of sheets due to its logarithmic component. However, only one of these sheets contains the eigenvalues k_n , satisfying Eq. (18), which correspond to the outgoing wave boundary conditions of RSs. This ‘physical’ sheet of $H_m(z)$ has a cut in the complex z -plane along the negative imaginary half-axis, as shown in Appendix B, which in turn gives rise to the same cut in the GF. Consequently, the Mittag-Leffler theorem used for the spectral representation of the GF needs to be modified to include the cut contribution, as done in Appendix B.

For the TM case treated here, the full GF of the homogeneous dielectric cylinder, which is defined via Maxwell’s equation with a line current source term, is given by $\hat{\mathbf{G}}_k = G_k \hat{\mathbf{z}} \otimes \hat{\mathbf{z}}$, in which

$$G_k(\boldsymbol{\rho}, \boldsymbol{\rho}') = \sum_m G_m(\rho, \rho'; k) \chi_m(\varphi) \chi_m(\varphi'), \quad (20)$$

and the radial components have the following spectral

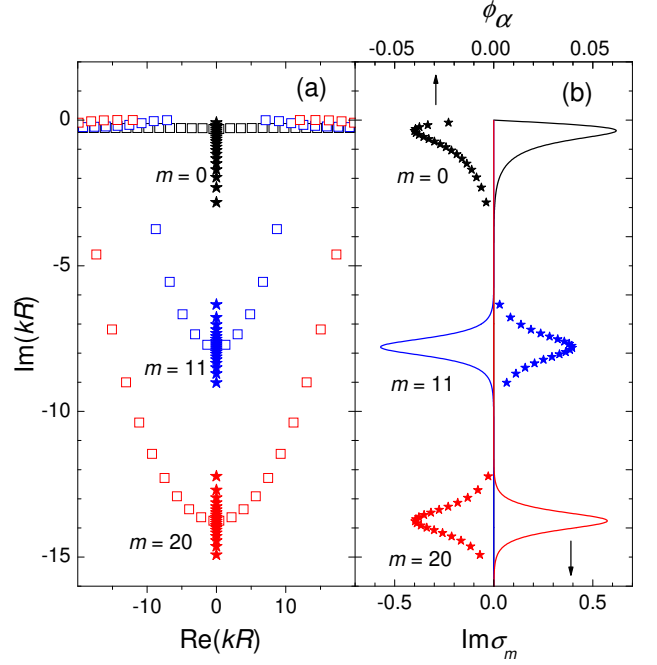


FIG. 1: (a): Cut poles k_α (stars) representing the cut of the GF of a homogeneous dielectric cylinder with $n_r = 2$, in the complex wave-number plane for $m = 0, 11$, and 20 . Normal poles k_n (open squares) are also shown. (b): Cut pole density $\sigma_m(k)$ (solid curves) and the cut pole strength $\phi_\alpha^{(m)}$ (stars), for the same values of m .

representation

$$\begin{aligned} G_m(\rho, \rho'; k) &= \sum_n \frac{R_m(\rho, k_n) R_m(\rho', k_n)}{2k(k - k_n)} \\ &+ \int_{-i\infty}^0 \frac{R_m(\rho, k') R_m(\rho', k')}{2k(k - k')} \sigma_m(k') dk' \\ &\equiv \oint_n \frac{R_m(\rho, k_n) R_m(\rho', k_n)}{2k(k - k_n)} \end{aligned} \quad (21)$$

derived in Appendix B. Note that the cut contribution to the GF spectrum in the form of the integral in the last equation is described in terms of the *same functions* as those used for discrete poles. This implies that the cut of the GF can be understood as a continuous distribution of additional poles along the negative imaginary half-axis with the density

$$\sigma_m(k) = \frac{4(n_r^2 - 1) J_m(n_r k R)}{\pi^2 k D_m^+(k R) D_m^-(k R)} \quad (22)$$

calculated in Appendix B. Here $D_m^\pm(z)$ are the two limiting values of $D_m(z')$ for z' approaching point z on the cut from its different sides $\text{Re } z' \gtrless 0$. Remarkably, the integrated density of the cut contribution to the GF is equivalent to half a normal pole: $\int_{-i\infty}^0 \sigma_m(k) dk = (-1)^{m+1}/2$.

To numerically treat the cut contribution in the linear eigenvalue problem Eq. (8), we discretize the integral in

Eq. (21) into a finite number of cut poles and add cut RSs to the basis. These cut poles have non-integer strength $\phi_\alpha^{(m)}$ determined by the cut pole density σ_m . The function $\sigma_m(k)$ is purely imaginary and is peaked close to normal poles k_n as can be seen in Fig. 1 for selected m . In the numerical calculations of the present work we have used cut pole positions and strengths determined by splitting the cut interval $[0, -i\infty]$ into $N_c^{(m)}$ regions $[q_\alpha^{(m)}, q_{\alpha+1}^{(m)}]$ numbered by $\alpha = 1, 2, \dots, N_c^{(m)}$, which are chosen to contain an equal weight according to

$$\int_{q_\alpha^{(m)}}^{q_{\alpha+1}^{(m)}} \sqrt{|\sigma_m(k)|} dk = \frac{1}{N_c^{(m)}} \int_{-i\infty}^0 \sqrt{|\sigma_m(k)|} dk. \quad (23)$$

For the numerical results shown later in this section and for the chosen values of $N_c^{(m)}$, using the weight $\sqrt{|\sigma_m|}$ in Eq. (23) was found to give the best accuracy of the RSE as compared to other powers of $|\sigma_m|$. Each region $[q_\alpha^{(m)}, q_{\alpha+1}^{(m)}]$ of the cut is represented by a cut pole of the GF at $k = k_\alpha^{(m)}$ given by the first moment,

$$k_\alpha^{(m)} = \int_{q_\alpha^{(m)}}^{q_{\alpha+1}^{(m)}} k \sigma_m(k) dk / \phi_\alpha^{(m)}, \quad (24)$$

where the cut pole strength $\phi_\alpha^{(m)}$ is defined as

$$\phi_\alpha^{(m)} = \int_{q_\alpha^{(m)}}^{q_{\alpha+1}^{(m)}} \sigma_m(k) dk. \quad (25)$$

An example of cut poles assigned for $m = 0, 11$, and 20 is given in Fig. 1(a). The cut poles contribute to the RSE in the same way as the normal poles, and the matrix elements with the cut RSs are given by the overlap integrals Eq. (D1) expressed in terms of exactly the same functions Eq. (16) as for the normal RSs. In discretization of the linear eigenvalue problem Eq. (8) of the RSE, the only modification caused by the cut is that the matrix of the perturbation is weighted according to the cut pole strengths $\phi_\alpha^{(m)}$, as described by Eq. (C7) in Appendix C.

In the numerical calculation, the total number of poles N_t used in Eq. (8) determines the computational complexity of the matrix eigenvalue problem, so that we are interested in the number of cut poles in the basis producing the best accuracy for a given N_t . We have investigated this numerically for the examples given below, and found that this is achieved using about 20% cut poles in the basis. Only for the homogeneous perturbation in Sec. III A, we used $N_c^{(m)} \sim N^{(m)}$, where $N^{(m)}$ is the number of normal poles in the basis for the given m , in order to demonstrate the convergence towards the exact solution. For all other numerical results we used $N_c^{(m)} \sim 0.2N^{(m)}$.

The rest of this section discusses results of the RSE for different effective 2D systems. We consider a homogeneous dielectric cylinder of radius R and refractive index $n_r = 2$ ($\varepsilon = 4$) with different types of perturbations,

namely a homogeneous perturbation of the whole cylinder in Sec. III A, a half-cylinder perturbation in Sec. III B, a thin-film perturbation in Sec. III C and a wire perturbation in Sec. III D. Explicit forms of the matrix elements for these perturbations and details of their calculation are given in Appendix D.

A. Homogeneous Cylinder Perturbation

The perturbation we consider in this section is a homogeneous change of ε over the whole cylinder, given by

$$\Delta\varepsilon(\rho, \varphi) = \Delta\varepsilon\theta(R - \rho) = \begin{cases} \Delta\varepsilon & \text{for } \rho \leq R, \\ 0 & \text{for } \rho > R \end{cases} \quad (26)$$

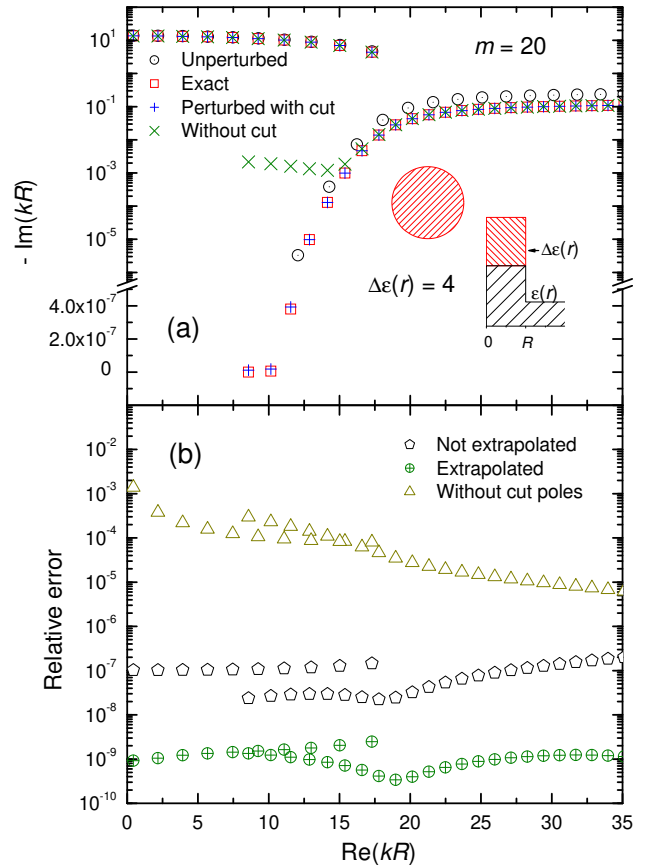


FIG. 2: (a): Perturbed RS wave numbers for the homogeneous perturbation Eq. (26) calculated via the RSE with $N = 800$ (only sine modes are shown). The perturbed poles with (+) and without (×) the cut contribution are compared with the exact solution (open squares). Unperturbed wave numbers are also shown (open circles with dots). Inset: Dielectric constant profile for the unperturbed and perturbed systems. (b): Relative error in the calculated perturbed wave numbers with (heptagons) and without (triangles) contribution of the cut. Relative error for a simulation including the cut and improved by extrapolation is also shown (crossed circles).

with the strength $\Delta\epsilon = 4$ used in the numerical calculation. For φ -independent perturbations, modes with different azimuthal number m are decoupled, and so are even and odd (cosine and sine) modes given by Eq. (14). We show only the sine modes here, and use for illustration $m = 20$. The matrix elements of the perturbation are calculated analytically and given by Eqs. (D3) and (D4). The homogeneous perturbation does not change the symmetry of the system, so that the perturbed modes obey the same secular equation Eq. (18) with the refractive index n_r of the cylinder changed to $\sqrt{n_r^2 + \Delta\epsilon}$, and thus the perturbed wave numbers κ_ν calculated using the RSE can be compared with the exact values $\kappa_\nu^{(\text{exact})}$.

We choose the basis of RSs for the RSE in such a way that for the given azimuthal number m and the given number of normal RSs N we find all normal poles $|k_n| < k_{\text{max}}(N)$ with a suitably chosen maximum wave vector $k_{\text{max}}(N)$ and then add the cut poles. We find that as we increase N , the relative error $|\kappa_\nu/\kappa_\nu^{(\text{exact})} - 1|$ decreases as N^{-3} . Following the procedure described in Ref. 32 we can extrapolate the perturbed wave numbers. The resulting perturbed wave numbers are shown in Fig. 2. The perturbation is strong, creating 3 additional WGMs with $m = 20$ having up to 4 orders of magnitude narrower linewidths. For $N = 800$, the RSE reproduces about 100 modes to a relative error in the 10^{-7} range, which is decreasing by one or two orders of magnitude after extrapolation. The contribution of the cut is significant: Ignoring the cut leads to a relative error of the poles in the 10^{-3} range. The fact that the relative error improves by 4-5 orders of magnitude after taking into account the cut in the form of the cut poles shows the validity of the reported analytical treatment of cuts in the RSE, and the high accuracy of the discretization method into cut poles.

B. Half-Cylinder Perturbation

We now consider a bulk perturbation which mixes modes with different m . The perturbation is given by

$$\Delta\epsilon(\rho, \varphi) = \Delta\epsilon \theta(R - \rho) \times \begin{cases} 1 & \text{for } |\varphi| \leq \pi/2, \\ -1 & \text{otherwise.} \end{cases} \quad (27)$$

In our numerical simulation we take $\Delta\epsilon = 0.2$. The matrix elements of the perturbation are given by Eqs. (D5)–(D7) which require a numerical integration. Owing to the symmetry of the perturbation, the sine and cosine basis modes are still de-coupled, therefore we treat them separately, see panels (a) and (b) in Fig. 3. Due to a relatively small perturbation (compared to that considered in Sec. III A), the mode positions in the spectrum do not change much. However, the quality factors Q of all WGMs decrease, as the lifetime of the resonances is now limited by an additional scattering at the step in the dielectric constant of the perturbed cylinder.

To the best of our knowledge, an analytic solution for this perturbation is not available and thus we cannot calculate the relative error of the RSE result with respect to the exact solution. However, we can investigate the convergence of the method in order to demonstrate how the RSE works in this case which is not reducible to an effective one-dimensional problem. This is done in Fig. 3 showing the perturbed sine and cosine modes for two different values of basis size N and in Fig. 4 where absolute errors M_ν are shown for several different values of N . Following Ref. 32, the absolute error is defined here as $M_\nu = \max_{i=1,2,3} |\kappa_\nu^{N_4} - \kappa_\nu^{N_i}|$, where $\kappa_\nu^{N_i}$ are the RS wave numbers calculated for basis sizes of $N_1 \approx N/2$, $N_2 \approx N/\sqrt{2}$, $N_3 \approx N/\sqrt[4]{2}$, and $N_4 = N$. The results for the cosine and sine modes are quite similar. From Fig. 4 we see that the perturbed resonances are converging with increasing basis size. Though, the absolute error has some fluctuations within an order.

We were able to see the power law of the convergence,

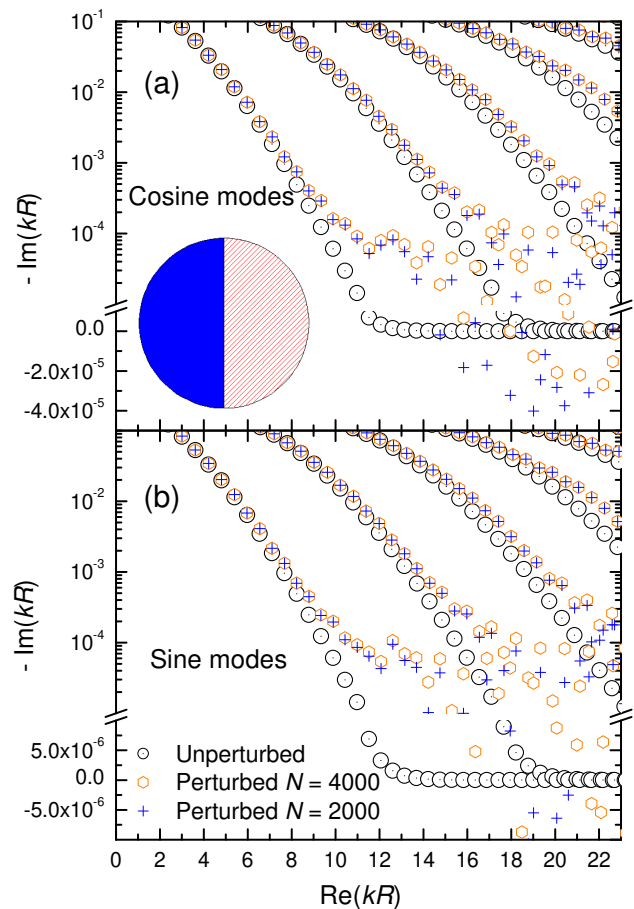


FIG. 3: Unperturbed (open circles with dots) and perturbed RS wave numbers of (a) cosine and (b) sine modes of a cylinder for a half-cylinder perturbation Eq. (27) with $\Delta\epsilon = 0.2$ and the basis sizes $N = 2000$ (crosses) and $N = 4000$ (hexagons). Only the WGM region is shown. Inset: Diagram showing the regions of increased (solid blue) and decreased (red and white striped) dielectric constant.

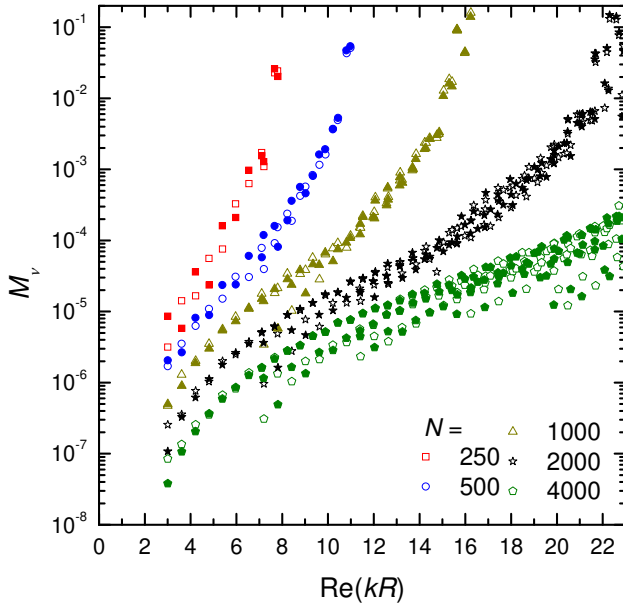


FIG. 4: Absolute errors M_ν of the RS wave numbers x_ν for the half-cylinder perturbation Eq. (27) as functions of $\text{Re } x_\nu$, calculated via the RSE for different basis sizes N , for cosine (closed shapes) and sine (open shapes) modes.

in agreement with Ref. 32, and found that the power law exponent is approximately -2 . We found however that owing to the above mentioned fluctuations, the power law convergence is not well developed compared to the one-dimensional problems considered so far (including the example of Sec. III A). Increasing the basis size N improves the power-law convergency. This is attributed to the larger number of basis states below a given $|k_{\max}R|$ in effective 2D systems compared to effective 1D systems. Thus one needs a larger basis in order to approximate discrete steps of the basis size by a continuous power law.

To show how a particular perturbed state is created as superposition of unperturbed states, we show by a star in Fig. 5 one the perturbed WGMs of Fig. 3 (a) which, owing to the perturbation, increases its linewidth by nearly an order of magnitude. The contribution of the basis states is visualized by circles of a radius proportional to $|c_{n\nu}|^{1/3}$, which are centered at the positions of the wave vectors k_n in the complex k -plane. The expansion coefficients $c_{n\nu}$ decrease quickly with the distance to the spectral position of the perturbed mode x_ν , with the dominant contribution coming from the nearest unperturbed RS, a typical feature of perturbation theory in closed systems. Importantly, this demonstrates that if we are interested in the modes within a small spectral region, we can limit the basis in the RSE to states close to that region. This result is crucial for the application of the RSE to effective 3D systems which have even larger numbers of basis states below a given $|k_{\max}R|$, as one can significantly reduce the number of basis states needed to calculate the perturbation of a mode of interest to a given accuracy.

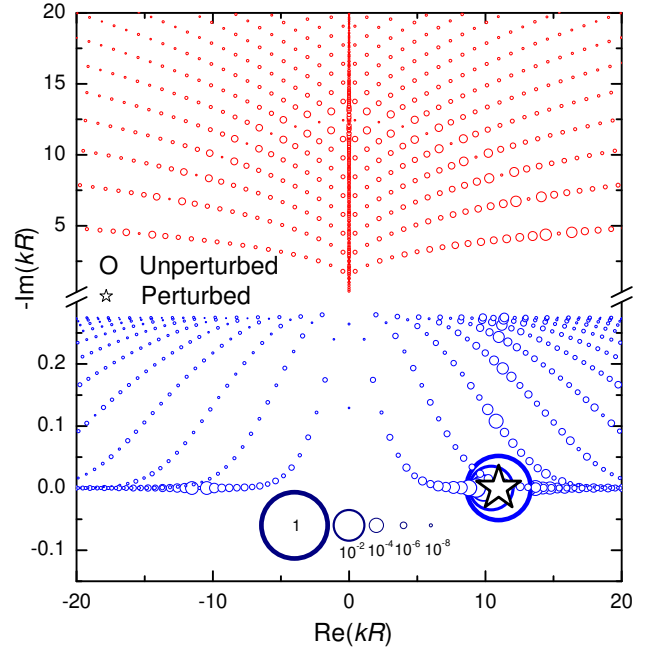


FIG. 5: Contributions of the basis RSs (black circles) to a given perturbed RS (blue star), calculated for the cosine modes and the half-cylinder perturbation Eq. (27), using $N = 4000$. All circles and the star are centered at the positions of the corresponding RS wave numbers in the complex k -plane. The radius of the black circles is proportional to $|c_{n\nu}|^{1/3}$. A key showing the relationship between circle radius and $|c_{n\nu}|^2$ is given by the red circles.

C. Thin-Film Perturbation

We now move from the bulk perturbations towards the case of a thin film embedded in the cylinder, corresponds to a line perturbation in the effective 2D system. The perturbation we consider in this section is given by

$$\Delta\epsilon(\rho, \varphi) = h\Delta\epsilon \frac{\theta(R - \rho)}{\rho} \delta(\varphi), \quad (28)$$

see the inset in Fig. 6. In our numerical simulation we take the strength of the perturbation $h\Delta\epsilon = -0.1R$. Physically this perturbation corresponds to a thin metal film of uniform negative dielectric constant $n_r^2 + \Delta\epsilon$ and width h much narrower than the shortest wavelength in the basis. The perturbation leaves the sine modes of the unperturbed cylinder unchanged. Hence we only include cosine modes into the basis. The perturbation matrix elements are given by Eq. (D8).

To our knowledge an analytic solution for this perturbation is not known and we therefore calculate the absolute error as in Sec. III B. Fig. 6 shows the resulting RS wave numbers and absolute errors for this thin-film perturbation. We see in Fig. 6(b) that the convergence of the RSE is slower than in the case of the half-moon perturbation. This is expected as the thin film has no geometrical effect on the wave-vector k_y , giving higher

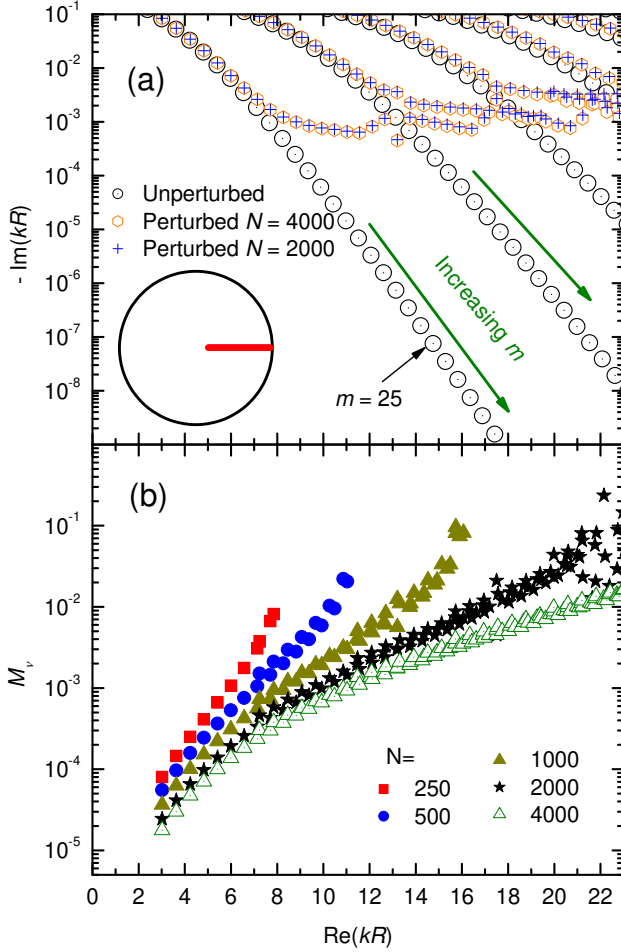


FIG. 6: (a): Unperturbed and perturbed RS wave numbers of cosine modes for a thin-film perturbation given by Eq. (28) with $h\Delta\epsilon = -0.1R$, calculated via the RSE with the basis sizes $N = 2000$ (crosses) and $N = 4000$ (hexagons). The unperturbed RSs are shown as open circles with dots. (b): Absolute errors M_v as functions of $\text{Re } \kappa_v$ calculated for different basis sizes N as labeled. Inset: Sketch showing the location of the thin metal film perturbation as a red line inside the unperturbed cylinder.

contributions of basis states with large k_y , similar to the results in 1D with a delta scatterer perturbation reported earlier.³² We have found that the power law exponent in this case is approximately -1 .

D. Thin-Wire Perturbation

As last example we consider a dielectric cylinder perturbed by a thin-wire perturbation which is represented by small disk of radius b centered at the point \mathbf{d} on the x -axis ($\varphi = 0$). We do not use here a delta perturbation, in order to compare it with an analytic solution available in the literature.³⁴ The perturbation is defined as

$$\Delta\epsilon(\rho) = \Delta\epsilon \theta(b - |\rho - \mathbf{d}|), \quad (29)$$

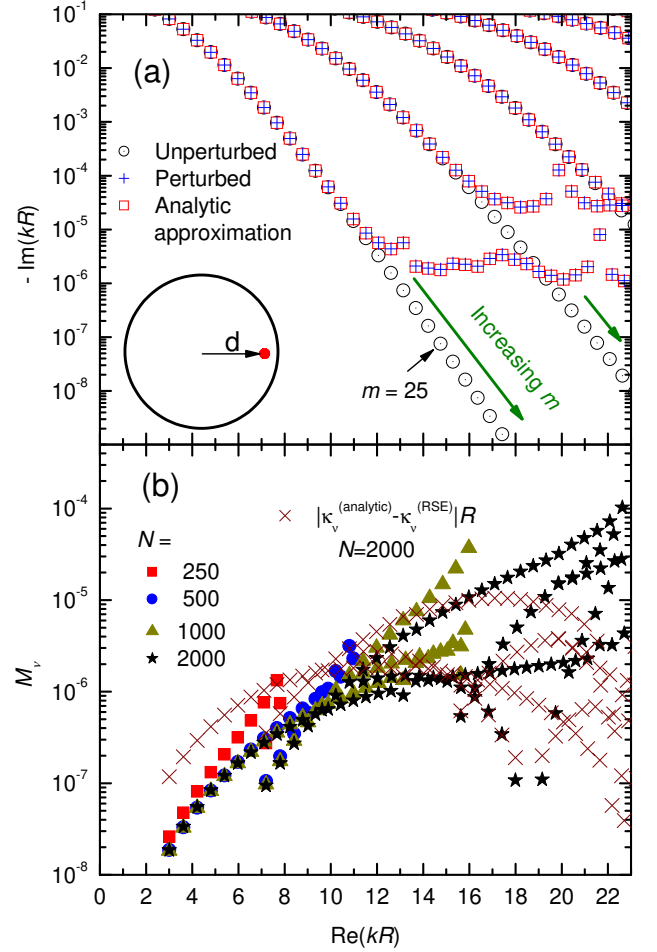


FIG. 7: (a): Unperturbed and perturbed RS wave numbers of cosine modes for a thin-wire perturbation given by Eq. (29) with $d = 0.8R$, $b = 0.001R$, and $\Delta\epsilon = 100$, calculated via the RSE with the basis size $N = 2000$ (crosses) and compared with the analytic approximation of Ref. 34 (empty squares). The unperturbed basis states are shown as open circles with dots. (b): Absolute errors M_v in RSE as functions of $\text{Re } \kappa_v$ calculated for different basis size N and the absolute difference between the RSE and the analytic approximation (crosses \times). Inset: Sketch showing the location of the wire as a red dot inside the unperturbed cylinder.

and we choose $d = |\mathbf{d}| = 0.8R$, $b = 0.001R$, and $\Delta\epsilon = 100$ (the unperturbed system is the same as before having $n_r = 2.0$). This perturbation leaves the sine and cosine modes decoupled, and the sine modes approximately unchanged (strictly for $d \rightarrow 0$). Therefore we show here the perturbation of the cosine modes. The RSE perturbation matrix elements are given by Eq. (D10). The resulting RS wave numbers are shown in Fig. 7(a) together with the analytic approximation, demonstrating a good agreement.

The absolute errors M_v are shown in Fig. 7(b). We see that the convergence in the case of a thin wire is even slower than for the thin-film perturbation shown in Sec. III C. This is expected as the thin wire has no

geometrical effect on both k_x and k_y , giving higher contributions of the basis states with large $|k|$. We found that within the basis sizes investigated, the power law is not well developed, but for weaker (smaller $|\Delta\epsilon|$) or more spatially extended (larger b) perturbations a better convergence is observed, as expected.

The analytic solution of Ref. 34 for a point-like scatterer in a 2D disk is not strict in any physical system. In the case of a delta scatterer, the secular equation is logarithmically divergent and thus cannot be used, while the accuracy of the model for a finite size scatterer relies on a number of approximations^{33,34} which require $|n_r \kappa_\nu b| \ll 1$, $|\kappa_\nu b \sqrt{n_r^2 + \Delta\epsilon}| \ll 1$, and also $|\text{Re } \kappa_\nu| \gg |\text{Im } \kappa_\nu|$, i.e. having a large Q . In addition to this, the point-like perturbation should not be too close to the edge of the disk, i.e. $|n_r \kappa_\nu (R - d)| \ll 1$. While we have chosen our parameters to be suitable for these approximations, we do not have a quantitative estimate of the error. Nevertheless, the comparison in Fig. 7 (a) of the RSE calculation with the analytic solution demonstrates a good agreement which is improving as we move closer to the origin in the complex k -plane, as detailed in Fig. 7 (b) where the absolute difference between the two calculations is shown.

IV. SUMMARY

We have applied the resonant state expansion (RSE) to effective two-dimensional (2D) open optical systems, such as dielectric micro-cylinders and micro-disks with perturbations. We have found and treated a cut of the Green's functions (GFs) of effective 2D systems – a feature which to our knowledge has not been mentioned in the literature but turned out to be crucial for the RSE as the states on the cut contribute to the completeness of the basis of RSs needed for the accuracy of the method. We have detailed the formulation of the RSE for a general 3D case taking into account the vectorial nature of the electro-magnetic field and tensor form of the GF and shown in detail how the theory is applied to effective 2D systems for which states on the cut are introduced and discretized for the numerics.

Using the analytically known basis of resonant states (RSs) of an ideal homogeneous dielectric cylinder – a complete set of eigenmodes satisfying outgoing wave boundary conditions – we have treated different types of perturbations, such as half-cylinder, thin-film and thin-wire perturbations. For all of these perturbations, the perturbed systems are not reducible to effective 1D ones, so that the present work demonstrates the applicability of the RSE to general effective 2D perturbations which mix all basis modes. We investigated the convergency for these perturbations and compared the RSE results, where it was possible, with available analytic solutions. In particular, we have made such a comparison for a homogeneous perturbation of a cylinder, which is reducible to an effective 1D system, and for point-like perturba-

tion of a disk which presents an essentially 2D system with mixing of all kind of modes in the given polarization of light. In both situation we have found agreement between the RSE and the known analytic solutions.

Acknowledgments

M. D. acknowledges support by EPSRC under the DTA scheme.

Appendix A: Spectral representation of the Green's function of an open system

The Green's function (GF) of an open electromagnetic system is a tensor $\hat{\mathbf{G}}_k$ which satisfies the outgoing wave boundary conditions and the Maxwell wave equation (1) with a delta function source term,

$$-\nabla \times \nabla \times \hat{\mathbf{G}}_k(\mathbf{r}, \mathbf{r}') + k^2 \varepsilon(\mathbf{r}) \hat{\mathbf{G}}_k(\mathbf{r}, \mathbf{r}') = \hat{\mathbf{1}} \delta(\mathbf{r} - \mathbf{r}'), \quad (\text{A1})$$

where $\hat{\mathbf{1}}$ is the unit tensor and $k = \omega/c$ is the wave vector of the electro-magnetic field in vacuum determined by the frequency ω , which can be real or complex. Physically, the GF describes the response of the system to a point current with frequency ω , i.e. an oscillating dipole. Using the reciprocity theorem,⁴² the relation

$$\mathbf{d}_1 \hat{\mathbf{G}}_k(\mathbf{r}_1, \mathbf{r}_2) \mathbf{d}_2 = \mathbf{d}_2 \hat{\mathbf{G}}_k(\mathbf{r}_2, \mathbf{r}_1) \mathbf{d}_1 \quad (\text{A2})$$

holds for any two dipoles $\mathbf{d}_{1,2}$ at points $\mathbf{r}_{1,2}$ oscillating with the same frequency. Therefore $\hat{\mathbf{G}}_k(\mathbf{r}, \mathbf{r}')$ is a symmetric tensor. Assuming a simple-pole structure of the GF with poles at $k = q_n$ and taking into account its large- k vanishing asymptotics, the Mittag-Leffler theorem^{43,44} allows us to express the GF as

$$\hat{\mathbf{G}}_k(\mathbf{r}, \mathbf{r}') = \sum_n \frac{\hat{\mathbf{Q}}_n(\mathbf{r}, \mathbf{r}')}{k - q_n}. \quad (\text{A3})$$

Substituting this expression into Eq. (A1) and convoluting with an arbitrary finite field $\mathbf{D}(\mathbf{r})$ over a finite volume V we obtain

$$\sum_n \frac{-\nabla \times \nabla \times \mathbf{F}_n(\mathbf{r}) + k^2 \varepsilon(\mathbf{r}) \mathbf{F}_n(\mathbf{r})}{k - q_n} = \mathbf{D}(\mathbf{r}),$$

where $\mathbf{F}_n(\mathbf{r}) = \int_V \hat{\mathbf{Q}}_n(\mathbf{r}, \mathbf{r}') \mathbf{D}(\mathbf{r}') d\mathbf{r}'$. Taking the limit $k \rightarrow q_n$ yields

$$-\nabla \times \nabla \times \mathbf{F}_n(\mathbf{r}) + q_n^2 \varepsilon(\mathbf{r}) \mathbf{F}_n(\mathbf{r}) = 0.$$

Due to the convolution with the GF, $\mathbf{F}_n(\mathbf{r})$ satisfies the same outgoing wave boundary conditions Eq. (2). Then, according to Eq. (1), $\mathbf{F}_n(\mathbf{r}) \propto \mathbf{E}_n(\mathbf{r})$ and $q_n = k_n$. Note that the convolution of the kernel $\hat{\mathbf{Q}}_n(\mathbf{r}, \mathbf{r}')$ with different functions $\mathbf{D}(\mathbf{r})$ can be proportional to one and the same

function $\mathbf{E}_n(\mathbf{r})$ only if the kernel has the form of a direct product:

$$\hat{\mathbf{Q}}_n(\mathbf{r}, \mathbf{r}') = \mathbf{E}_n(\mathbf{r}) \otimes \mathbf{E}_n(\mathbf{r}')/w_n, \quad (\text{A4})$$

in which the vectorial nature of the field and the symmetry of the kernel Eq. (A2) were taken into account and a normalization constant w_n was introduced. The direct vector product \otimes is defined as $\mathbf{c}(\mathbf{a} \otimes \mathbf{b})\mathbf{d} = (\mathbf{c} \cdot \mathbf{a})(\mathbf{b} \cdot \mathbf{d})$, for any vectors \mathbf{a} , \mathbf{b} , \mathbf{c} , and \mathbf{d} .

The asymptotics of the GF for $k \rightarrow \infty$ following from Eq. (A1) requires that $\hat{\mathbf{G}}_k \propto k^{-2}$, which for the spectral representation Eq. (A3) provides the sum rule:⁴⁴

$$\sum_n \hat{\mathbf{Q}}_n(\mathbf{r}, \mathbf{r}') = 0. \quad (\text{A5})$$

Using Eq. (A4) and Eq. (A5), together with Eq. (A3) yields

$$\hat{\mathbf{G}}_k(\mathbf{r}, \mathbf{r}') = \sum_n \frac{\mathbf{E}_n(\mathbf{r}) \otimes \mathbf{E}_n(\mathbf{r}')}{k(k - k_n)} \frac{k_n}{w_n}. \quad (\text{A6})$$

The normalization constants w_n can be determined from the normalization condition Eq. (4). We have shown for specific systems with analytic solutions³¹ that

$$w_n = 2k_n. \quad (\text{A7})$$

These systems were 1D or 3D with spherical symmetry, where the normalization constants w_n have the meaning of the Wronskian derivatives at $k = k_n$. The derivation for 2D systems with cylindrical symmetry is similar. However a specific property of 2D systems is the presence of a continuum in the RS spectrum, which is a cut of the GF in the complex k -plane. The spectral representation of the GF includes this cut contribution as integral:

$$\hat{\mathbf{G}}_k(\mathbf{r}, \mathbf{r}') = \oint_n \frac{\mathbf{E}_n(\mathbf{r}) \otimes \mathbf{E}_n(\mathbf{r}')}{2k(k - k_n)}. \quad (\text{A8})$$

The cut is discussed in more detail in Sec. III and in Appendix B, where we also show the validity of Eq. (A7) for a homogeneous cylinder.

Substituting the GF of Eq. (A8) into Eq. (A1) and using the sum rule Eq. (A5) leads to the closure relation

$$\frac{\varepsilon(\mathbf{r})}{2} \oint_n \mathbf{E}_n(\mathbf{r}) \otimes \mathbf{E}_n(\mathbf{r}') = \hat{\mathbf{1}}\delta(\mathbf{r} - \mathbf{r}') \quad (\text{A9})$$

which expresses the completeness of the RSs, so that any function can be written as a superposition of RSs including the contribution of the cut. Due to the surface term in the orthogonality condition Eq. (3), RSs form an over-complete basis,^{45,46} i.e. any RS wave function $\mathbf{E}_n(\mathbf{r})$ can be written as a superposition of the wave functions of other RSs of the basis.

Appendix B: Green's function of a homogeneous cylinder

The TM component of the GF of a homogeneous cylinder in vacuum satisfies the following equation

$$\left[\nabla_\rho^2 + \varepsilon(\rho)k^2 \right] G_k(\rho, \rho') = \delta(\rho - \rho') \quad (\text{B1})$$

with

$$\varepsilon(\rho) = \begin{cases} n_r^2 & \text{for } \rho \leq R, \\ 1 & \text{for } \rho > R. \end{cases} \quad (\text{B2})$$

Using the angular basis Eq. (14) the GF can be written as

$$G_k(\rho, \rho') = \frac{1}{\sqrt{\rho\rho'}} \sum_m \tilde{G}_m(\rho, \rho'; k) \chi_m(\varphi) \chi_m(\varphi'), \quad (\text{B3})$$

similar to Eq. (20). Note that we redefined here the radial part as $\tilde{G}_m(\rho, \rho'; k) = \sqrt{\rho\rho'} G_m(\rho, \rho'; k)$ which satisfies

$$\left[\frac{d^2}{d\rho^2} - \frac{m^2 - 1/4}{\rho^2} + k^2 \varepsilon(\rho) \right] \tilde{G}_m(\rho, \rho'; k) = \delta(\rho - \rho'). \quad (\text{B4})$$

Using two linearly independent solutions $f_m(\rho)$ and $g_m(\rho)$ of the corresponding homogeneous equation which satisfy the asymptotic boundary conditions

$$\begin{aligned} f_m(\rho) &\propto \rho^{m+1/2} & \text{for } \rho \rightarrow 0, \\ g_m(\rho) &\propto e^{ik\rho} & \text{for } \rho \rightarrow \infty. \end{aligned}$$

the GF can be expressed as

$$\tilde{G}_m(\rho, \rho'; k) = \frac{f_m(\rho_{<})g_m(\rho_{>})}{W(f_m, g_m)}, \quad (\text{B5})$$

in which $\rho_{<} = \min\{\rho, \rho'\}$, $\rho_{>} = \max\{\rho, \rho'\}$, and the Wronskian $W(f, g) = fg' - f'g$. For TM polarization, a suitable pair of solutions is given by

$$\begin{aligned} f_m(\rho) &= \sqrt{\rho} \cdot \begin{cases} J_m(n_r \rho), & \rho \leq R, \\ a_m J_m(\rho) + b_m H_m(\rho), & \rho > R, \end{cases} \\ g_m(\rho) &= \sqrt{\rho} \cdot \begin{cases} c_m J_m(n_r \rho) + a_m H_m(n_r \rho), & \rho \leq R, \\ H_m(\rho), & \rho > R, \end{cases} \end{aligned}$$

where

$$\begin{aligned} a_m(k) &= [n_r J'_m(n_r x) H_m(x) - J_m(n_r x) H'_m(x)] \pi i x / 2, \\ b_m(k) &= [J'_m(x) J_m(n_r x) - n_r J_m(x) J'_m(n_r x)] \pi i x / 2, \\ c_m(k) &= [H'_m(x) H_m(n_r x) - n_r H_m(x) H'_m(n_r x)] \pi i x / 2 \end{aligned}$$

with $x = kR$. The Wronskian is calculated to be

$$W(f_m, g_m) = 2ia_m(k)/\pi = -xD_m(x),$$

with $D_m(x)$ defined in Eq. (19). Inside the cylinder, the GF then takes the form

$$\begin{aligned} \tilde{G}_m(\rho, \rho'; k) &= \frac{\pi}{2i} \sqrt{\rho\rho'} \left[J_m(n_r k \rho_{<}) H_m(n_r k \rho_{>}) \right. \\ &\quad \left. + \frac{c_m(k)}{a_m(k)} J_m(n_r k \rho_{<}) J_m(n_r k \rho_{>}) \right]. \quad (\text{B6}) \end{aligned}$$

The GF has simple poles k_n in the complex k -plane which are the wave vectors of RSs, given by $a_m(k_n) = 0$, a equation equivalent to Eq.(18). The residues Res_n of the GF at these poles are calculated using

$$r_m(k_n) = \left. \frac{c_m(k)}{\frac{d}{dk}a_m(k)} \right|_{k=k_n} = \frac{2ik_n}{\pi(n_r^2 - 1)[k_n R J_m(n_r k_n R)]^2} \quad (\text{B7})$$

In addition to the poles, the GF has a cut in the complex k -plane along the negative imaginary half-axis. The cut is due to the Hankel function $H_m(z)$ which describes the field outside the cylinder and contributes to Eqs. (16) (18) and Eq.(B6), and is not uniquely defined. Indeed it can be expressed as⁴⁷

$$H_m(z) = J_m(z) + iN_m(z), \quad (\text{B8})$$

using a multiple-valued Neumann function

$$N_m(z) = \tilde{N}_m(z) + \frac{2}{\pi} J_m(z) \ln \frac{z}{2}, \quad (\text{B9})$$

where $\tilde{N}_m(z) = z^m F_m(z^2)$ is a single-valued polynomial⁴⁷ while $\ln z$ is a multiple-valued function defined on an infinite number of Riemann sheets. We have verified that only one such sheet provides the asymptotics $H_m(z) \propto \exp(iz)/\sqrt{z}$ for $z \rightarrow \infty$, which is required for the RS wave functions outside the cylinder to satisfy the outgoing wave boundary conditions Eq. (2). This ‘physical’ sheet has a cut going from the branch point at $z = 0$ to infinity, and the position of the cut is not arbitrary. To find the cut position let us use the symmetry of the RS wave numbers, $k_{-n} = -k_n^*$, discussed in Sec.II. Let us also, using properties of cylindrical functions,^{47,48} bring the secular equation (18) to the form

$$J_{m+1}(n_r z) H_{m-1}(z) = J_{m-1}(n_r z) H_{m+1}(z), \quad (\text{B10})$$

in which $z = k_n R$. We note that if $z = k_n R$ is a complex solution of Eq. (B10), then $-z^*$ is also a solution of the same equation. We take two equations, one is the conjugate of Eq. (B10) and the other is Eq. (B10) itself but taken with the argument $-z^*$, and add them up. Substituting there Eqs. (B8) and (B9) and using the facts that⁴⁷

$$\begin{aligned} [J_m(z)]^* &= J_m(z^*) = (-1)^m J_m(-z^*), \\ [\tilde{N}_m(z)]^* &= \tilde{N}_m(z^*) = (-1)^m \tilde{N}_m(-z^*), \end{aligned}$$

we arrive at the condition

$$\ln(-z^*) - (\ln z)^* = \pi i, \quad (\text{B11})$$

which is fulfilled, for any z , only if $\ln z$ [and consequently $H_m(z)$] has a cut along the negative imaginary half-axis.

Owing to the cut of the Hankel function $H_m(z)$ the GF also has a cut along the negative imaginary half-axis in the complex k -plane, so that on both sides of the

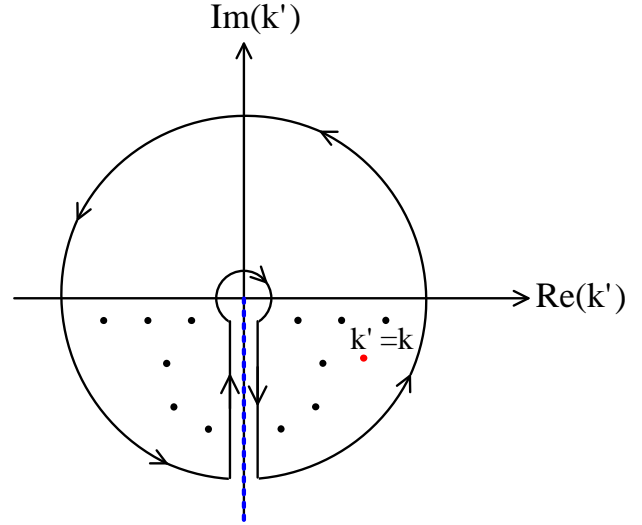


FIG. 8: Sketch showing the contour of integration in Eq. (B14) as well as poles (black dots) and the cut (blue dashed line) of the GF in the complex k' -plane. An extra pole at $k' = k$ is shown by a red dot.

cut \tilde{G}_m takes different values: \tilde{G}_m^+ on the right-hand side and \tilde{G}_m^- on the left-hand side of the cut. The step $\Delta\tilde{G}_m = \tilde{G}_m^+ - \tilde{G}_m^-$ over the cut can be calculated using the corresponding difference in the Hankel function:

$$\Delta H_m(z) = H_m^+(z) - H_m^-(z) = 4J_m(z).$$

The result is

$$\Delta\tilde{G}_m(\rho, \rho'; k) = \frac{\pi}{2i} \sqrt{\rho\rho'} J_m(n_r k \rho_{<}) J_m(n_r k \rho_{>}) \Delta Q_m(k) \quad (\text{B12})$$

where

$$\Delta Q_m(k) = \left[4 + \frac{c_m^+}{a_m^+} - \frac{c_m^-}{a_m^-} \right] = - \left(\frac{4}{\pi k R} \right)^2 \frac{1}{D_m^+(k) D_m^-(k)} \quad (\text{B13})$$

with $D_m(k)$ given by Eq. (19).

Let us now use the residue theorem for the function $\tilde{G}_m(\rho, \rho'; k')/(k - k')$ integrating it in the complex k' -plane along a closed contour consisting of three parts, see Fig. 8: A large counter-clockwise circumference with a radius tending to infinity, two straight lines circumventing the cut and approaching it from both sides, and a small clockwise circumference around the origin with a radius tending to zero. Since the GF behaves as k^{-2} at large values of k and takes finite values or logarithmically diverges at $k = 0$, both large- and small-circle integrals vanish, so that the only remaining integrals are those which are taken along the cut:

$$\begin{aligned} \oint \frac{\tilde{G}_m(\rho, \rho'; k')}{k - k'} dk' &= \int_0^{-i\infty} \frac{\tilde{G}_m^+ dk'}{k - k'} + \int_{-i\infty}^0 \frac{\tilde{G}_m^- dk'}{k - k'} \\ &= 2\pi i \sum_n \frac{\text{Res}_n}{k - k_n} - 2\pi i \tilde{G}_m(\rho, \rho'; k). \end{aligned} \quad (\text{B14})$$

Note that in second part of the above equation we have made use of the residue theorem, expressing the closed-loop integral in the left-hand side in terms of a sum over residues at all poles inside the contour. Using Eq. (B14) the GF can be expressed as

$$\tilde{G}_m(\rho, \rho'; k) = \sum_n \frac{\text{Res}_n}{k - k_n} + \frac{1}{2\pi i} \int_{-i\infty}^0 \frac{\Delta \tilde{G}_m(\rho, \rho'; k') dk'}{k - k'}, \quad (\text{B15})$$

which is a generalization of the Mittag-Leffler theorem. This is used in Sec. III when applying the RSE to 2D systems with a cut of their GF. The residues Res_n of the GF contributing to Eq. (B15) are calculated as

$$\text{Res}_n = \frac{\pi}{2i} \sqrt{\rho \rho'} J_m(n_r k \rho_{<}) J_m(n_r k \rho_{>}) r_m(k_n), \quad (\text{B16})$$

with $r_m(k_n)$ found in Eq. (B7). Given that the spatial dependence of the GF, as described by Eqs. (B15), (B16), and (B12), is represented by products of the RS wave functions $R_m(\rho, k_n)$ and their analytic continuations $R_m(\rho, k)$ with k -values taken on the cut, we arrive at the GF in the form of Eqs. (21) and (22) which are then used in the RSE.

Appendix C: RSE with a cut

This section provides some details on how the RSE can be used in practice when the GF has a cut, and in particular, how the cut discretization, producing cut poles, modifies the linear matrix eigenvalue problem Eq. (8), the central equation of the RSE.

To make our consideration as general as possible we use the 3D version of the Dyson equation (5) as a starting point and substitute into it spectral representations Eq. (A6) of the unperturbed and perturbed GFs. Equating the residues at the perturbed poles (i.e. integrating along the infinitesimal circumference around each pole) we obtain³¹

$$\mathcal{E}_\nu(\mathbf{r}) = \oint_n \frac{\mathbf{E}_n(\mathbf{r}) \int \mathbf{E}_n(\mathbf{r}') \cdot \mathcal{E}_\nu(\mathbf{r}') \Delta \varepsilon(\mathbf{r}') d\mathbf{r}'}{2(k_n/\kappa_\nu - 1)}, \quad (\text{C1})$$

where both pole and cut contributions are included. The cut has a continuous contribution. Therefore, in numerical calculation, we discretize the cut representing it by a finite number of cut poles chosen in an optimum way as described in Sec. III. For an arbitrary function $F(k)$,

$$\oint_n F_n \equiv \sum_n F(k_n) + \int_{-i\infty}^0 F(k) \sigma(k) dk \approx \sum_{\bar{n}} F_{\bar{n}} \phi_{\bar{n}} \quad (\text{C2})$$

where the combined index \bar{n} is used to denote both real poles k_n and cut poles k_α simultaneously. The weighting factors $\phi_{\bar{n}}$ come from the weight function $\sigma(k)$ introduced in Eq. (22) and are defined as follows

$$\phi_{\bar{n}} = \begin{cases} \phi_n = 1 & \text{for real poles,} \\ \phi_\alpha & \text{for cut poles,} \end{cases} \quad (\text{C3})$$

where

$$\phi_\alpha = \int_{q_\alpha}^{q_{\alpha+1}} \sigma(k) dk \quad (\text{C4})$$

is an integral of the weight function over an interval $[q_\alpha, q_{\alpha+1}]$ within which a cut pole k_α is chosen. The method of choosing this interval and the positions of the cut poles specific to this work are described in Sec. III, by Eqs. (23) and (24). Note that we have dropped here the azimuthal index m for simplicity, however the discretization of the cut is generally different for different m leading to m -dependent cut poles and their weighting factors $\phi_{\bar{n}}$.

Now, discretizing Eq. (C1) in accordance with Eq. (C2), substituting the expansion

$$\mathcal{E}_\nu(\mathbf{r}) = \oint_n b_{n\nu} \mathbf{E}_n(\mathbf{r}) \approx \sum_{\bar{n}} \phi_{\bar{n}} b_{\bar{n}\nu} \mathbf{E}_{\bar{n}}(\mathbf{r}) \quad (\text{C5})$$

of the perturbed RS wave function into it, and equating coefficients at the same basis functions, we obtain

$$b_{\bar{n}\nu} = \frac{1}{2(k_{\bar{n}}/\kappa_\nu - 1)} \sum_{\bar{n}'} \phi_{\bar{n}'} b_{\bar{n}'\nu} V_{\bar{n}\bar{n}'} . \quad (\text{C6})$$

Introducing new expansion coefficients

$$c_{\bar{n}\nu} = b_{\bar{n}\nu} \sqrt{\frac{k_{\bar{n}}}{\phi_{\bar{n}} \kappa_\nu}},$$

the matrix eigenvalue problem takes the form

$$\sum_{\bar{n}'} \left(\frac{\delta_{\bar{n}\bar{n}'}}{k_{\bar{n}}} + \frac{V_{\bar{n}\bar{n}'}}{2} \sqrt{\frac{\phi_{\bar{n}} \phi_{\bar{n}'}}{k_{\bar{n}} k_{\bar{n}'}}} \right) c_{\bar{n}'\nu} = \frac{1}{\kappa_\nu} c_{\bar{n}\nu}, \quad (\text{C7})$$

which is a discretized version of Eq. (8). The matrix elements $V_{\bar{n}\bar{n}'}$ are defined by Eq. (9) with \bar{n} and \bar{n}' numbering both normal and cut poles. They are calculated below in Appendix D for various types of perturbation.

Appendix D: Matrix elements for various perturbations in 2D

In this section we give explicit expressions for the matrix elements $V_{\bar{n}\bar{n}'}$ of the specific perturbations considered in this paper. As a starting point we use the following general formula for the matrix elements of an arbitrary perturbation $\Delta \varepsilon(\rho, \varphi)$ inside the cylinder of radius R :

$$V_{\bar{n}\bar{n}'} = \int_0^{2\pi} \chi_m(\varphi) \chi_{m'}(\varphi) d\varphi \times \int_0^R \Delta \varepsilon(\rho, \varphi) R_m(\rho, k_{\bar{n}}) R_{m'}(\rho, k_{\bar{n}'}) \rho d\rho, \quad (\text{D1})$$

in which R_m and χ_m are the eigenfunctions of the homogeneous cylinder given by Eqs. (14)–(17).

1. Homogeneous cylinder perturbation

The homogeneous perturbation Eq. (26) does not mix different m -values. The matrix elements between RS with the same azimuthal number m are given by the radial overlap integrals

$$V_{\bar{n}\bar{n}'} = \Delta\epsilon \int_0^R R_m(\rho, k_{\bar{n}}) R_m(\rho, k_{\bar{n}'}) \rho d\rho \quad (D2)$$

yielding for identical basis states ($\bar{n} = \bar{n}'$)

$$V_{\bar{n}\bar{n}} = \frac{\Delta\epsilon}{n_r^2 - 1} \left[1 - \frac{J_{m-1}(n_r k_{\bar{n}} R) J_{m+1}(n_r k_{\bar{n}} R)}{[J_m(n_r k_{\bar{n}} R)]^2} \right] \quad (D3)$$

and for different basis states ($\bar{n} \neq \bar{n}'$)

$$V_{\bar{n}\bar{n}'} = \frac{\Delta\epsilon}{n_r^2 - 1} \frac{2}{n_r R (k_{\bar{n}}^2 - k_{\bar{n}'}^2)} \times \left[k_{\bar{n}'} \frac{J_{m-1}(n_r k_{\bar{n}'} R)}{J_m(n_r k_{\bar{n}'} R)} - k_{\bar{n}} \frac{J_{m-1}(n_r k_{\bar{n}} R)}{J_m(n_r k_{\bar{n}} R)} \right]. \quad (D4)$$

2. Half-cylinder perturbation

The most efficient way of calculating the matrix elements of the perturbation Eq. (27) is to calculate the angular parts of the integrals analytically and the radial parts numerically. The matrix elements have the form

$$V_{\bar{n}\bar{n}} = \Delta\epsilon P_{mm'} Q_{k_{\bar{n}} k_{\bar{n}'}}, \quad (D5)$$

in which the angular overlap integrals $P_{mm'}$ are vanishing when taken between modes of different parity, i.e. between sine and cosine modes, see Eq. (14), and between same parity modes corresponding to azimuthal numbers m and m' of different parity. The non-vanishing integrals are given by

$$P_{mm'} = \int_{-\pi/2}^{\pi/2} \chi_m(\varphi) \chi_{m'}(\varphi) d\varphi - \int_{\pi/2}^{3\pi/2} \chi_m(\varphi) \chi_{m'}(\varphi) d\varphi \\ = s_m s_{m'} (\psi_{m-m'} \pm \psi_{m+m'}) \quad (D6)$$

with $+$ ($-$) corresponding to cosine (sine) modes and s_m and ψ_m defined as

$$s_m = \begin{cases} \pi^{-1/2} & \text{for } m \neq 0, \\ (2\pi)^{-1/2} & \text{for } m = 0, \end{cases} \\ \psi_m = [1 - (-1)^m] \frac{\sin(m\pi/2)}{m}.$$

The radial part of the matrix elements of the perturbation is given by the integrals

$$Q_{kk'}^{mm'} = \int_0^R R_m(\rho, k) R_{m'}(\rho, k') \rho d\rho \quad (D7) \\ = \frac{2}{R^2(n_r^2 - 1)} \frac{\int_0^R J_m(n_r k \rho) J_{m'}(n_r k' \rho) \rho d\rho}{J_m(n_r k R) J_{m'}(n_r k' R)}$$

which we calculate numerically.

3. Thin-film perturbation

The matrix elements of the perturbation Eq. (28) are given by the integrals

$$V_{\bar{n}\bar{n}'} = h \Delta\epsilon \chi_m^2(0) \int_0^R R_m(\rho, k_{\bar{n}}) R_{m'}(\rho, k_{\bar{n}'}) d\rho, \quad (D8)$$

similar to Eq. (D7), which are calculated numerically.

4. Thin-wire perturbation

The RSE perturbation matrix elements for this system are calculated by summing I same-strength delta scatterers on a square grid covering a circle. The perturbation Eq. (29) is thus modeled by

$$\Delta\epsilon \approx \Delta\epsilon \frac{\pi b^2}{I} \sum_{i=1}^I \frac{1}{\rho} \delta(\rho - \rho_i) \delta(\varphi - \varphi_i). \quad (D9)$$

The matrix elements then have the form

$$V_{\bar{n}\bar{n}'} = \Delta\epsilon \frac{\pi b^2}{I} \sum_{i=1}^I E_{\bar{n}}(\rho_i, \varphi_i) E_{\bar{n}'}(\rho_i, \varphi_i) \quad (D10)$$

with $E_{\bar{n}}(\rho, \varphi)$ given by Eq. (13).

* egor.muljarov@astro.cf.ac.uk; on leave from General Physics Institute RAS, Moscow, Russia.

¹ K. Vahala, *Nature* **424**, 839 (2003).

² *Optical Processes in Microcavities*, Editors: R. K. Chang

and A. J. Campillo, (World Scientific, Singapore, 1996).

³ P. Russell, *Science* **299**, 358 (2003).

⁴ L. Collot, V. Lefèvre-Seguin, B. Brune, J. M. Raimond, and S. Haroche, *Europhys. Lett.* **23**, 327 (1993).

- ⁵ S. L. McCall, A. F. J. Levi, R. E. Slusher, S. J. Pearton, and R. A. Logan, *Appl. Phys. Lett.* **60**, 289 (1992).
- ⁶ B. Gayral, J.M. Gerard, A. Lemaitre, C. Dupuis, L. Manin, and J. L. Pelouard, *Appl. Phys. Lett.*, **75**, 1908 (1999).
- ⁷ L. Chantada, N. I. Nikolaev, A. L. Ivanov, P. Borri, and W. Langbein, *J. Opt. Soc. Am. B.* **25** 1312 (2008).
- ⁸ R. Dubertrand, E. Bogomolny, N. Djellali, M. Lebental, and C. Schmit, *Phys. Rev. A* **77**, 013804 (2008).
- ⁹ C. P. Dettmann, G. V. Morozov, M. Sieber, and H. Waalkens, *Europhys. Lett.* **87**, 34003 (2009)
- ¹⁰ F. Vollmer and S. Arnold, *Nat. Methods* **5**, 591 (2008).
- ¹¹ J. Lutti, W. Langbein, and P. Borri, *Appl. Phys. Lett.* **93**, 151103 (2008).
- ¹² J. Zhu, S. K. Ozdemir, Y. F. Xiao, L. Li, L. N. He, D. R. Chen, and L. Yang, *Nat. Photonics* **4**, 46 (2010).
- ¹³ T. J. Kippenberg, *Nat. Photonics* **4**, 9 (2010).
- ¹⁴ N. Noto, F. Vollmer, D. Keng, I. Teraoka and S. Arnold, *Opt. Lett.* **30**, 510, (2005).
- ¹⁵ F. Vollmer, S. Arnold, D. Braun, I. Teraoka, and A. Libshaber, *Biophys. J.*, **85**, 1974 (2003).
- ¹⁶ F. Vollmer, and D. Braun, A. Libchaber, M. Khoshshima, I. Teraoka, and S. Arnold, *Appl. Phys. Lett.* **80**, 4057 (2002).
- ¹⁷ M. Rosenblit, P. Horak, S. Helsenby, and R. Folman, *Phys. Rev. A* **70**, 053808 (2004).
- ¹⁸ S. I. Shopova, R. Rajmangal, S. Holler, and S. Arnold, *Appl. Phys. Lett.* **98**, 243104 (2011).
- ¹⁹ L. He, S. K. Özdemir, J. Zhu, W. Kim, and L. Yang, *Nat. Nanotech.* **6** 428 (2011).
- ²⁰ N. C. Frateschi and A. F. J. Levi, *Appl. Phys. Lett.* **66** 2932 (1995); *J. Appl. Phys.* **80**, 644 (1996).
- ²¹ V. Sandoghdar, F. Treussart, J. Hare, V. Lefèvre-Seguin, J. -M. Raimond, and S. Haroche, *Phys. Rev. A* **54**, 1777 (1996).
- ²² V. S. Ilchenko and A. B. Matsko, *IEEE J. Sel. Top. Quantum Electron* **12**, 15 (2006).
- ²³ Q. J. Wang, C. Yan, N. Yu, J. Unterhinninghofen, J. Wiersig, C. Pflügl, L. Diehl, T. Edamura, M. Yamanishi, H. Kan, F. Capasso, *Proc. Nat. Acad. Sci. USA* **107**, 22407 (2010).
- ²⁴ A. Taflove, S. C. Hagness, *Computational electrodynamics: the finite-difference time-domain method*, 2nd ed. (Artech House, Norwood, MA, 2000).
- ²⁵ S. C. Hagness, D. Rafizadeh, S. T. Ho, and A. Taflove, *J. Lightwave Technol.* **15**, 2154 (1997).
- ²⁶ J. Wiersig, *J. Opt. A: Pure Appl. Opt.* **5**, 53 (2003).
- ²⁷ O.C. Zienkiewicz and R.L. Taylor, *The finite element method*, 5th ed. Butterworth Heinemann, 2000.
- ²⁸ B. M. A. Rahman, F. A. Fernandez, and J. B. Davies, *Proc. IEEE* **79**, 1442 (1991).
- ²⁹ B. N. Jiang, J. Wu, and L. Povinelli, *J. Comp. Phys.* **125** 104, (1996).
- ³⁰ A. V. Boriskin, S. V. Boriskina, A. Rolland, R. Sauleau, and A. I. Nosich, *J. Opt. Soc. Am. A* **25**, 1169 (2008).
- ³¹ E. A. Muljarov, W. Langbein, and R. Zimmermann, *Europhys Lett.* **92**, 50010 (2010).
- ³² M. Doost, W. Langbein, and E. A. Muljarov, *Phys. Rev. A* **85**, 023835 (2012).
- ³³ C. P. Dettmann, G. V. Morozov, M. Sieber, and H. Waalkens, *Europhys. Lett.* **82**, 34002 (2008).
- ³⁴ C. P. Dettmann, G. V. Morozov, M. Sieber, and H. Waalkens, *Phys. Rev. A* **80**, 063813 (2009).
- ³⁵ M. Neviere, in *Electromagnetic Theory of Gratings*, edited by R. Petit (Springer-Verlag, Berlin, 1980).
- ³⁶ R. W. Wood, *Phil. Mag.* **4**, 396 (1902).
- ³⁷ J. W. S. Rayleigh, *Phil. Mag.* **14**, 60 (1907).
- ³⁸ U. Fano, *J. Opt. Soc. Am.* **31**, 213 (1941).
- ³⁹ A. Hessel and A. A. Oliner, *Appl. Opt.* **4**, 1275 (1965).
- ⁴⁰ A. B. Akimov, N. A. Gippius, S. G. Tikhodeev, *Pis'ma Zh. Eksp. Teor. Fiz.* **93**, 473 (2011) [*JETP Lett.* **93**, 427 (2011)].
- ⁴¹ For details and derivation see Ref. 31 and Appendix C.
- ⁴² M. Born and E. Wolf, *Principles of Optics*, 7th edition (Cambridge University Press, 1999), page 423.
- ⁴³ R. M. More, *Phys. Rev. A* **4**, 1782 (1971).
- ⁴⁴ J. Bang and F. A. Gareev, *Lett. Nuovo Cimento*, **32**, 420 (1981).
- ⁴⁵ G. García-Calderón, *Lett. Nuovo Cimento*, **33**, 253 (1982).
- ⁴⁶ P. Lind, *Phys. Rev. C* **47**, 1903 (1993).
- ⁴⁷ I. S. Gradshteyn and I. M. Ryzhik, *Table of Integrals, Series, and Products* (Academic Press, New York, 1965).
- ⁴⁸ H. Bateman, *Higher Transcendental functions*, Vol. II (McGraw-Hill Book Company, 1953).